Molecular Dynamics Simulations of Polymers in Micro–environments

M. Kenward, F. Tessier, Y. Tatek, Y. Gratton, S. Guillouzic, and G. W. Slater[a]

[a]Department of Physics, University of Ottawa, 150 Louis Pasteur, Ottawa, ON, K1N 6N5,
gslater@science.uottawa.ca

We provide an overview of ongoing work using large scale Molecular Dynamics (MD) simulations to study systems comprising macromolecules and explicit fluid in various contexts relevant to emerging bioanalytical microdevices and single molecule manipulation techniques. In particular, we discuss the application of MD simulations to polymer translocation through a nanopore, electroosmotic flow control in small capillaries, polymer stretching, and polymer collisions with obstacles. We also present more fundamental applications of MD to the study of molecular-scale friction coefficients and planar perturbations in a fluid. The simultaneous increase in available computational resources and decrease in relevant system dimensions offers unprecedented opportunities to perform realistic simulations to refine our knowledge of these issues and guide future developments in this field.

Nous présentons un panorama de nos travaux basés sur la dynamique moléculaire (DM) à grande échelle appliquée à des systèmes comportant des macromolécules et des fluides dans divers contextes reliés aux dispositifs bioanalytiques en émergence ou aux techniques de manipulation de molécules individuelles. En particulier, nous discutons de l'application de la DM au déplacement d'un polymère à travers un nanopore, au contrôle d'écoulement électro-osmotique dans les capillaires, à l'étirement des polymères et aux collisions des polymères avec des obstacles. Nous présentons aussi des applications plus fondamentales de la DM à l'étude des coefficients de frottement à l'échelle moléculaire et aux perturbations planaires dans un fluide. L'augmentation de la puissance de calcul, combinée à la diminution de la taille des systèmes d'intérêt, nous permet d'effectuer des simulations réalistes et ainsi de raffiner notre compréhension du domaine et de guider les développements futurs.

1 Introduction

With the development of micro- and even nanofluidic devices, more robust modeling is required in order to understand observed behaviour in these systems. Many of the physical mechanisms involved have no macroscopic analogue and are ill understood. For example, there is a major effort to design and utilize microelectromechanical systems (MEMS) in a variety of situations ranging from diagnostic tools to smart materials, and in order to effectively do so we need to understand the dynamics of the components which constitute these devices. Of particular interest to our group are systems which incorporate polymeric materials, at either the micro- or nanoscale. In this paper we combine computer simulations and theoretical methods to examine the behaviour of polymers and other macromolecules in a number of model systems.

Large scale computer simulations which aim to explore mesoscale systems (with upwards of millions of particles), have become an invaluable research tool. Simulation methodologies including Monte Carlo [1,2], continuum models such as Navier-Stokes [3], coarse grained and atomistic Molecular Dynamics [4,5] and Brownian Dynamics are the most prevalent form of simulation for these types of systems. The simulation method used depends on a balance between the:

1. Required level of detail (e.g., length scales).
2. Time scales associated with observed behaviour.
3. Available computational resources.
4. Effort required for a timely implementation.

Figure 1 illustrates the level of detail and computational time of each method. For the particular systems we are examining, coarse grained Molecular Dynamics provides the most useful length and time scales, along with the preservation of hydrodynamics and the molecular properties of the system.

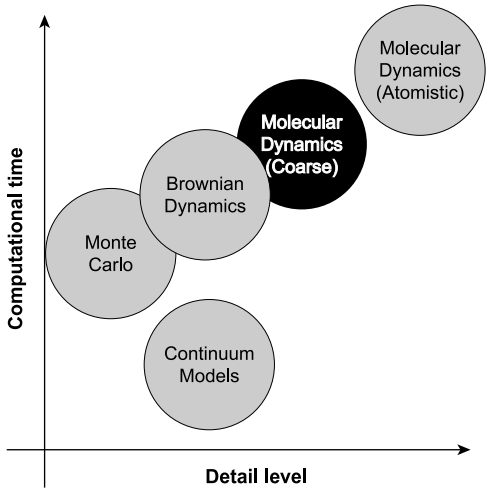

Figure 1. *Schematic illustration of several methods of simulation in terms of their relative computational time and level of detail.*

1.1 Molecular Dynamics: A brief overview

Since the aim of this paper is to illustrate the application of MD simulations to a variety of systems and not to provide a detailed description of Molecular Dynamics, we only give a brief overview and list appropriate references for the interested reader. In short, from the perspective of

a physicist, MD is the solution of the set of classical equations of motion for a fully interacting collection of objects (atoms for example) [6,5], i.e., the solution of the N-body equations of motion for a system.

Since in general this solution cannot be obtained analytically, we must resort to numerical solutions. This amounts to discretizing the equations of motion using an appropriate finite difference scheme. In particular we utilize a second order method (in time), referred to as the Velocity Verlet algorithm [5]. This method is both relatively straightforward to implement and also allows relatively large time steps δt. Moreover the Velocity Verlet algorithm is amenable to parallelization [6].

The systems we examine contain one or several of the following components: polymers, solvent, walls, charged species and external forces. One important addition to our simulations is the explicit inclusion of solvent and hence hydrodynamics. Although hydrodynamics is usually discussed in the guise of Navier-Stokes equations, its existence is really a molecular property of the system. Moreover it plays a crucial role in many phenomena at the microscopic and nanoscopic level, which may fall beyond the reach of a continuum description of fluid dynamics.

1.2 Model Fluid and Polymers

In this model we represent a single fluid particle as a soft sphere of radius $\sigma/2$ which interacts with other fluid particles via the Lennard-Jones potential given by

$$V_{\mathrm{LJ}}(r) = \begin{cases} 4\epsilon\left(\left(\frac{\sigma}{r}\right)^{12} - \left(\frac{\sigma}{r}\right)^{6}\right) + \epsilon, & r \le r_{\mathrm{c}} \\ 0, & r \ge r_{\mathrm{c}} \end{cases}$$

We further simplify by choosing $r_{\mathrm{c}} = 2^{1/6}\sigma$ and we therefore have a fluid with purely repulsive interactions. All distances are expressed in terms of σ, masses in terms of m, times in terms of $\tau = \sqrt{m\sigma^2/\epsilon}$ and velocities in terms of $v = \sqrt{\epsilon/m}$. For all of the simulations presented here we work in the micro-canonical ensemble at fixed reduced temperature $T^* = 1$, reduced density $\rho^* = 0.85$ and a time step of $\delta t = 0.005\tau$ unless otherwise specified.

A schematic illustration of a Lennard-Jones fluid particle and the first layer of solvent around it is shown in Figure 2 b). To illustrate the fluid like structure, Figure 3 shows the radial distribution function of a pure Lennard-Jones fluid. This radial distribution function is characteristic of a fluid local packing with peaks at $r \approx \sigma, 2\sigma, 3\sigma \ldots$

In order to model the polymers, we utilize a coarse grained approximation which replaces the real physical polymers with beads, representing one or many chemical units, and springs which represent the bonds between neighbouring units along a chain. The interactions between non-bonded beads along the chain are given by the Lennard-Jones potential whereas the bonded interactions are modeled via the Finitely Extensible Non-Linear Elastic (FENE) potential,

$$V_{\mathrm{FENE}}(r) = -\frac{k}{2}R_0^2 \ln\left(1 - \frac{r^2}{R_0^2}\right) \qquad (1)$$

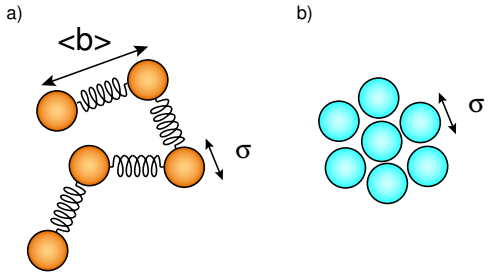

Figure 2. *Illustration of a) model polymers composed of Lennard Jones beads connected via FENE springs where $\langle b \rangle$ denotes the average bond length and σ the diameter of a bead b) model Lennard-Jones fluid particles with first layer of solvent.*

where R_0 is an upper bound on the bond distance and k is essentially a "spring constant" [5]. For more detailed descriptions and implementation details, the reader can consult references [6,7,5,8,9].

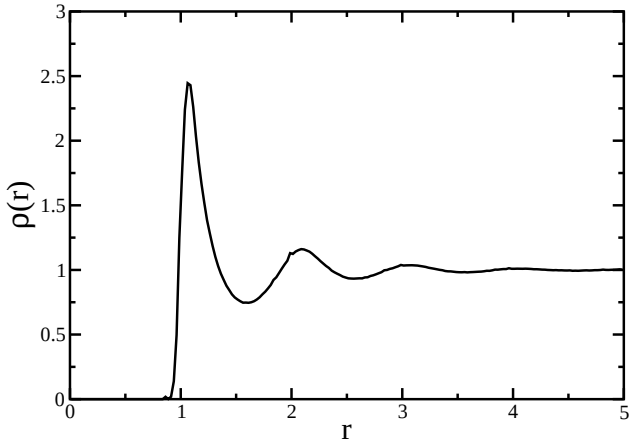

Figure 3. *Radial distribution function $\rho(r)$ for a pure Lennard-Jones fluid obtained from the MD simulations. Characteristic peaks are evident at $r \approx \sigma, 2\sigma, 3\sigma, \ldots$ corresponding to the first, second, third . . . solvent layers.*

Since our long term goal for these simulations is to examine mesoscopic and macroscopic systems with $> 10^6$ particles, we require the use of High Performance Computing resources such as those available via HPCVL (**www.hpcvl.org**). Parallelization of Molecular Dynamics simulations with short range interactions is typically done using either; so-called atom-, force-, and spatial-decomposition algorithms [10]. As such our next step will be the parallelization of the simulations using one of the above algorithms, in order to begin examining much larger systems.

1.3 Visualization Tools

Visualizing the results from a simulation provides not only an inherently useful debugging tool but also a physically intuitive way to examine a system and its proper-

ties. In this vein, we have developed some generic tools for the visualization of results from the Molecular Dynamics simulations. In particular we have written graphical interfaces, in **OpenGL**, which allow us to visualize our results in both real-time and post simulation modes. Snapshots from this Molecular Dynamics viewer are shown in Figure 4. Though there are similar tools openly available, our viewer has the advantage of being tailored for our specific project. Furthermore we can easily add, modify, and adapt this viewer for a number of distinct projects in our group.

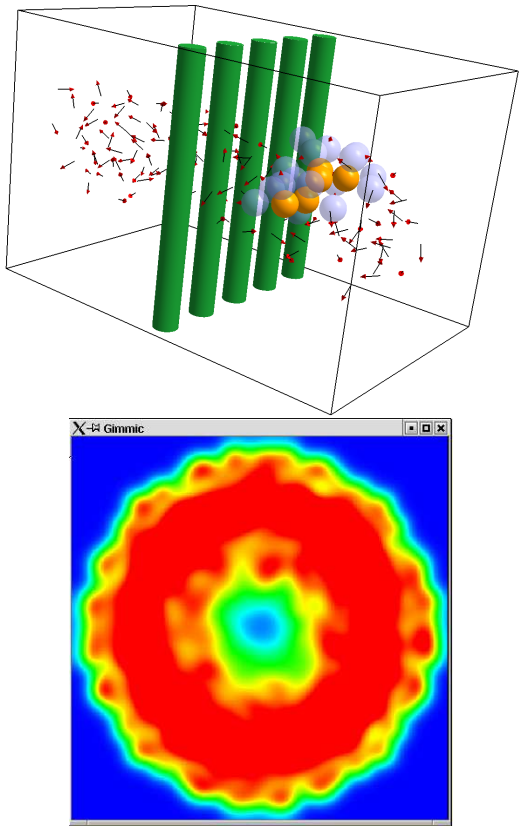

Figure 4. *Snapshots from our custom built Molecular Dynamics viewer, written in* **OpenGL**. *The top panel shows an image from a polymer–post collision simulation: the velocity field associated with a small volume of the fluid is illustrated by the small arrows. The bottom panel is a temperature plot of a cross–section of a capillary filled with a fluid.*

2 Molecular Dynamics: Applications and Examples

2.1 Polymer Translocation in Nanopores

The sequencing of the human genome has become one of the crowning achievements of human-kind. This information has the potential to lead to both better understanding and treatment of human diseases. Though the scientific community has managed to sequence a generic version of the genomic text, the ultimate goal is to sequence individual genomes in a short period of time (a few hours) which could allow for the diagnosis and prevention of diseases.

One promising sequencing method is the use of the translocation of single-stranded DNA molecules through a nanopore in a membrane or a solid surface [11–13]. As the polymer either diffuses or is pulled through the opening, the individual bases of the DNA strand can ideally be read, providing a tool for sequencing. This proposed method could potentially sequence the entire genome in minutes. In order to better understand the relevant physics, we have carried out MD simulations of polymer translocation. A schematic illustration of polymer diffusing through a nanopore is given in Figure 5.

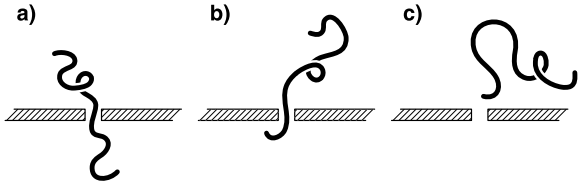

Figure 5. *Schematic illustration of a model polymer diffusing through a nanopore. a) The polymer is centered in the nanopore. b) The polymer begins to diffuse away from the pore. c) Eventually the polymer escapes.*

Our simulations consist of placing a polymer in a single void in a monolayer [111] face-centered cubic structure. We first let the polymer relax while fixing its center bead in the pore. After this relaxation period, we release the polymer and observe its behaviour, until it escapes.

A recent theory of Chuang *et. al.* [14] predicts the scaling behaviour of the mean end-to-end translocation time $\tau_{\rm trans}$ of a polymer through a nanopore. In 3D, with no external force and no hydrodynamics, it scales as $\tau_{\rm trans} \propto N^{2.2}$ while with hydrodynamics it scales as $\tau_{\rm trans} \propto N^{1.8}$ (where N is the number of monomers in the chain). Chuang *et. al.* [14] also predict that the variance of the translocation coordinate s scales as $\langle \Delta s^2 \rangle \propto t^{1.12}$ when hydrodynamic interactions are present and $\langle \Delta s^2 \rangle \propto t^{0.92}$ when they are not (where the translocation coordinate is the length of the polymer on a given side of the pore).

From the MD simulations we obtain

$$\langle \Delta s^2 \rangle \propto t^{0.918 \pm 0.016} \tag{2}$$

and

$$\tau_{\rm trans} \propto N^{\beta} \quad \text{with} \quad \beta \geq 2.27 \pm 0.04 \tag{3}$$

for the variance of the translocation coordinate and the mean escape times respectively. Although these results are preliminary, they agree nicely with the predictions of Chuang *et. al.* for translocation in the presence of excluded volume but with no hydrodynamic interactions. This seems to be reasonable since the presence of the wall is expected to screen hydrodynamic interactions to some extent [15].

2.2 Friction coefficients of Rigid Rods

A classic problem from fluid dynamics is determining the friction coefficient of an object. The so-called slen-

der body theory of Batchelor [16] provides well known results for friction coefficients of arbitrarily shaped objects. These results are obtained from the solution of Navier-Stokes equations for low Reynolds number flow subject to appropriate boundary conditions and typically for macroscopic objects. Though these results are known to be accurate for macroscopic systems, when the objects under consideration are on the same scale as the fluid particles, these results do not necessarily remain valid.

We use MD simulations to explore fluid behaviour and microscopic fluid dynamics of objects on the same scale as the fluid. We have carried out simulations which directly determine the friction coefficient of rigid rods composed of spheres. Further to this we can illustrate as the size of the object is decreased to the scale of the fluid particles, the friction coefficient does indeed reduce to that of a single solvent particle. Here we present the case for all particle sizes from the fluid scale to an object composed of 60 fluid size particles. Similar work has been done experimentally for chains of spheres composed of magnetically induced linear chains of super-paramagnetic particles, where the friction coefficient is measured during sedimentation [3,17], though the sphere size is much larger than the size of the fluid particles.

Slender body theory predicts friction coefficients ξ for rigid rods, moving either parallel $||$ or perpendicular $\perp$ to a field, of the form

$$\xi_{||}(L) = \frac{C\pi\eta L}{\ln(L/2b) + \gamma_{||}}, \quad \xi_{\perp}(L) = \frac{2C\pi\eta L}{\ln(L/2b) + \gamma_{\perp}} \tag{4}$$

where $C, \gamma_{\perp}$ and $\gamma_{||}$ are constants and η is the viscosity. The crucial thing to note is that this theory predicts the following relationship

$$\frac{\xi_{\perp}(L)}{\xi_{||}(L)} \approx 2 \tag{5}$$

Indeed, from the simulations we can recover this asymptotic behaviour and the crossover from microscopic to this large scale friction. Figure 6 illustrates the friction coefficients as a function of chain length and the ratio $\xi_{\perp}(L)/\xi_{||}(L)$. This illustrates that MD can be used to examine fluid dynamics starting from a non-continuum based description of the fluid. As we begin to examine larger systems, with on the order of millions of particles we can further examine the crossover from microscopic single particle fluid dynamics to mesoscopic and ideally macroscopic fluid behaviour.

2.3 Polymer–Obstacles Collisions

Another field where the use of computer simulations may reap many benefits is that of separation science, i.e., the separation of DNA, or other polymers by mass, charge or shape. Typically polydisperse solutions of polymers are separated using either gel or capillary electrophoresis [18–20]. A better understanding of the dynamics of polymers in microenvironments can lead to both optimized and novel methods of separating DNA. One such method is the use

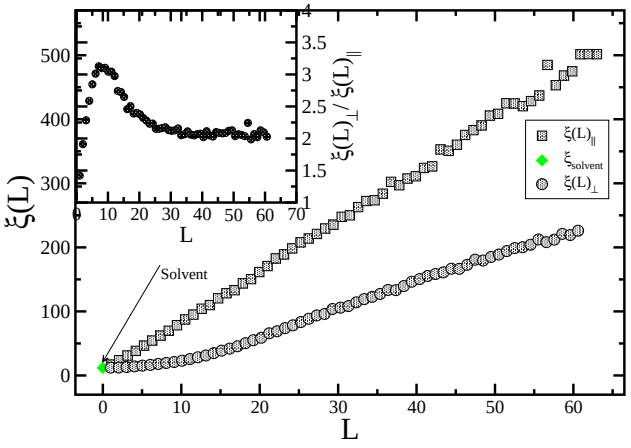

Figure 6. *Friction coefficients for a chain of spheres moving perpendicular $\xi_{\perp}(L)$ and parallel $\xi_{||}(L)$ to an applied field. Inset figure is the ratio of $\xi_{\perp}(L)$ to $\xi_{||}(L)$ as a function of L. Clearly the ratio tends asymptotically to a value of 2, as predicted by slender-body theory.*

of self-assembled arrays of paramagnetic obstacles created by the application of a magnetic field to a suspension of super paramagnetic particles confined between layers of glass [21]. This results in the formation of small quasi-regular arrays of posts (or obstacles) which can serve as a sieve to separate polymer. Such as system has been designed, built and used effectively to separate double-stranded DNA by Doyle *et. al.* [21].

In such a system, the polymers migrate under the presence of an external electric field. They consequently collide with posts, are deformed and form pulley like structures. The release time of the polymer is dictated by its length and a competition between the opposing arms of the pulley like conformation which results. One of the long standing questions is to what degree does the presence of hydrodynamics dictate the release time of the polymer [22,23].

We have carried out extensive MD simulations which examine this process. Figure 7 shows a snapshot from one of the simulations, illustrating a collision and release of a polymer. Using these simulations we can effectively carry out an autopsy of the collision dynamics of a single polymer chain with a post. Figure 8 shows the position of center of mass of a single polymer chain as it undergoes a collision with a post in the MD simulation. From this we can generate a good qualitative model of the behaviour of a polymer during collision. The polymer moves through the solvent with constant velocity v_0, until the center of mass is within about R_g of the post, it is then deformed by the presence of the post and later becomes trapped. There is a competition between the two arms of the resultant pulley like structure which forms, the longer arm winning. This results in the eventual release of the polymer. At this point, it accelerates and returns to a random walk conformation and eventually reaches constant velocity v_0 again.

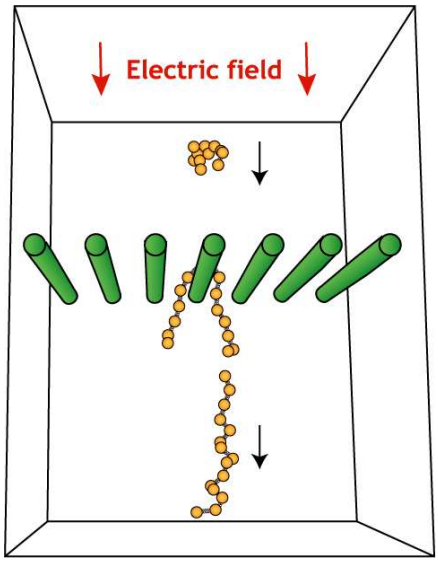

Figure 7. *Illustration of a polymer post collision sequence from the MD simulations.*

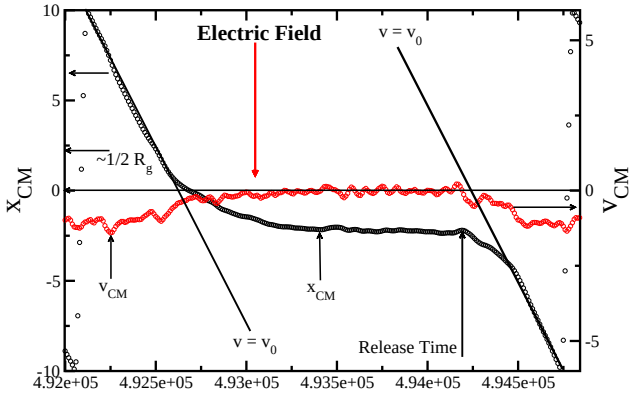

Figure 8. *Instantaneous position x_{CM} and velocity of the center of mass v_{CM} of a polymer before, during and after a collision with a post.*

2.4 MD simulations of Electroosmotic Flow

Electroosmotic flow (EOF) refers to a fluid flow induced by an external electric field applied along a solid surface, and occurs when a space charge builds up in the fluid near the surface [24]. This interfacial charge may arise for different reasons, a common one being the dissociation of chemical groups from the solid and the ensuing accumulation of counterions or ions from the solution in an electrical double-layer (EDL) near the surface [25]. When an external electric field is applied parallel to the surface, this layer of mobile charges is set in motion and eventually drags the bulk of the fluid by viscosity into a flow with a flat profile (a so-called *plug flow*, see Figure 9). Hence EOF serves as a very efficient fluid transport mechanism in small capillaries [26]. Calculations based on mean-field arguments have been used time and again to characterize the EOF in various geometries, including channels with rectangular cross-section, cylindrical capillaries and narrow slits, in steady-state, transient, and oscillating regimes [27,28,26,29–31].

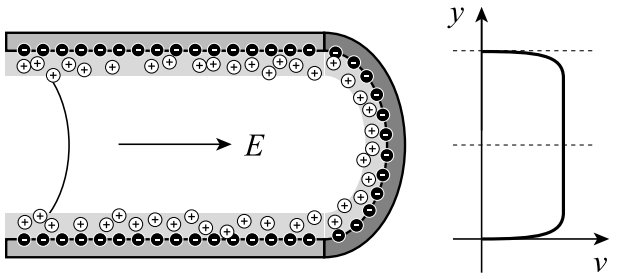

Figure 9. *Schematic representation of EOF generation inside a cylindrical capillary. Bound charges on the wall surface induce a net charge layer in the fluid. Upon the application of an external field, this mobile layer is set in motion, and eventually drags the whole fluid into a plug flow with a flat profile, depicted schematically on the right.*

The typical approach to treat this problem analytically or numerically is to consider on one hand the Poisson equation for the electrostatic potential $\phi(\mathbf{r})$ at position $\mathbf{r}$ in the system, and on the other hand the Boltzmann distribution for the density of mobile ions in the solution in terms of the valence z_k and the bulk concentration $n_{k\mathrm{o}}$ of each of the N ionic species [24]. These two expressions together yield the well-known Poisson-Boltzmann (PB) equation for $\phi(\mathbf{r})$ in a polyelectrolyte solution at thermal equilibrium:

$$\nabla^2\phi(\mathbf{r}) = -\frac{e}{4\pi\varepsilon_{\mathrm{o}}\varepsilon}\sum_{k=1}^{N} z_k n_{k\mathrm{o}}\, e^{-ez_k\phi(\mathbf{r})/k_{\mathrm{B}}T}\,, \qquad (6)$$

where ε_{o} and ε are the permittivity of the vacuum and the relative permittivity of the fluid, e is the elementary charge, and $k_{\mathrm{B}}T$ is a measure of the mean thermal energy. With appropriate boundary conditions, we can solve equation (6) numerically for any geometry, and by substituting the results in a finite difference Navier-Stokes equation solver we can obtain the flow field induced by the EOF, in both transient and steady-state regimes. Analytical work is also possible, albeit with a linearized version of equation (6) and for simple geometries only.

Despite all the knowledge gained in this way over the last thirty years, revisiting EOF with Molecular Dynamics simulations is interesting and important for two main reasons. First, as modern analytical chemistry devices shrink to the micrometer and even to the nanometer scale, the validity of the continuum picture of hydrodynamics itself becomes questionable. In particular, the correct representation of the velocity field near the fluid-solid interface (e.g. *slip* vs. *no-slip* boundary condition) becomes critical in devices so small that the *bulk* of the fluid lies, in fact, near a solid surface. Secondly, we want to study surface modification using polymer molecules grafted or adsorbed on the capillary wall. Such polymer coatings are of great industrial interest, especially for the control of EOF in bioanalytical microdevices [32]. However the complexity of the system is such that we cannot hope to describe it accurately

within a model based on equation (6). Molecular Dynamics simulation, a firmly established and robust method to study fluids, electrolytes, macromolecules, etc., stands as a natural choice for a realistic investigation of EOF.

Studying EOF requires that we add charged species in our simulations. Long-range electrostatic forces generally pose problems because of interactions between ions in different periodic images, although robust schemes based on Ewald summations have been developed [33–35]. However, our narrow capillary here is essentially one-dimensional on large length scales and we can include electrostatics directly, provided that the periodic box is long enough. We moderate Joule heating inside the system by controlling the temperature of the wall. The first object of our investigation is the distribution of ions which we will compare with that predicted by equation (6), as we vary the capillary diameter and the ionic strength of the buffer solution. Further on, we will add an external electric field and study the transient and steady state EOF flows. Assuming we reproduce EOF correctly, we can then include grafted or adsorbed polymer chains on the wall to gain a sound understanding of their effect on EOF.

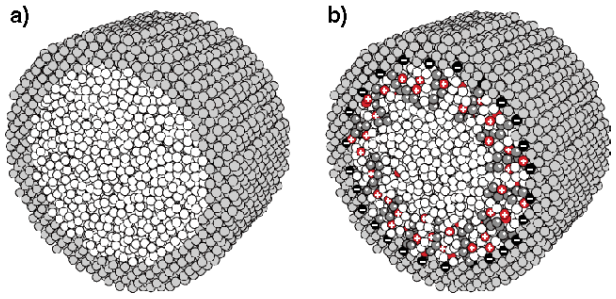

Figure 10. *a) A snapshot from an MD simulation of a short section of a capillary filled with fluid. b) A mock-up of the simulation of* EOF *control using polymer coatings we are setting out to perform, complete with polymer chains, ions on the capillary walls and counterions in solution.*

2.5 Stretching Single Polymers

Understanding the properties of single linear chains in good solvent is important to better describing single chains in microenvironments. With the development of techniques such as optical tweezers and single molecule fluorescence spectroscopy it is now possible to experimentally manipulate and observe single polymer chains. This technology enables us to stretch a DNA molecule and measure forces on the order of femtonewtons! One of the most useful analytical tools for examining polymers is the scaling theory developed by de Gennes [36]. In essence, this theory utilizes the fact that all properties in the system can be related to some universal scale (for example a length scale) such as the mean squared end-to-end distance $\langle h^2 \rangle$.

This section presents a brief overview of two simple models: the Freely Jointed Chain (FJC) and the Rouse model applied to the stretching of a single polymer [36–38]. At first glance, a polymer looks like a random walk (RW) where every monomer is subjected to Brownian motion caused by the surrounding solvent. From this observation, a simplistic model can describe the polymer as a series of links of fixed length b (the Kuhn length) which allow all possible orientations. In RW theory, it is a well known fact that for a chain of N links, the mean squared end-to-end distance $\langle h^2 \rangle$ is

$$\langle h^2 \rangle = Nb^2 \tag{7}$$

The Rouse model consists of a series of beads connected by springs [37]. Compared with the FJC model, the Rouse model re-groups $n < N$ links to form a spring. These Gaussian springs have an elastic constant of $K_n = 3k_BT/nb^2$ and a mean squared end-to-end distance $\langle b_n^2 \rangle = nb^2$. The n links in a spring produce $M = N/n$ springs connecting $M+1$ beads. The Rouse chain conserves $\langle h^2 \rangle$:

$$\langle h^2 \rangle = M\langle b_n^2 \rangle = Mnb^2 = Nb^2 \tag{8}$$

One caveat in the Rouse model is the spring constant: it does not accurately model the finite extensibility of a real chain. A polymer will always have a maximum extension after which it will break. We need a more realistic spring constant which ensures finite extension of the chain while keeping the mean value fixed. One possibility is to use the Finitely-Extensible Nonlinear Elastic (FENE) model. It is important to note that these models do not take into account either the presence of a solvent (hydrodynamic effects) or excluded volume interactions.

There are two ways to describe polymer stretching: the stress and the strain ensemble. In the stress ensemble, an external force is applied to the ends of the chain. The strength of this force is fixed to $\pm f$ but the ends are able to move freely. One can then calculate the mean end-to-end distance $\langle h(F) \rangle$. It is given by [39]

$$\frac{\langle h(F) \rangle}{h_{\max}} \approx \coth(F) - \frac{1}{F} \tag{9}$$

For $F \gg 1$,

$$\frac{\langle h(F) \rangle}{h_{\max}} \simeq 1 - \frac{1}{F} \tag{10}$$

where $F = fb/k_BT$ is the scaled force. Note that for $F \gg 1$, $\langle h \rangle$ tends to $h_{\max} = Nb$. A polymer in the strain ensemble has it ends fixed in space and the force felt by the ends F(h) is measured. We do not discuss the strain ensemble here.

To understand the stretching of real chains, one must incorporate excluded volume interactions, i.e., those interactions which prohibit any two monomers from occupying the same volume of space. Excluded volume interactions tend to swell the polymer compared to the FJC model. Inclusion of excluded volume in theoretical calculations is highly non-trivial. The MD simulations implicitly include all of the aforementioned effects and allow us to analyze chain stretching with excluded volume and hydrodynamics.

The stretching of single polymer chains is classified by four distinct regimes. Figure 11 illustrates these four regimes along with the associated scaling relationships for the mean squared end-to-end distance. We have successfully used Molecular Dynamics simulations to investigate and recover known force extension relationships of single isolated polymers in the strong stretching regime of the stress ensemble, i.e., Figure 11 c). We have also determined the difference between the stress and strain ensembles along with examining the relaxation of a polymer following the removal of the forces $\pm F$. In the latter case, hydrodynamics leads to highly nontrivial effects.

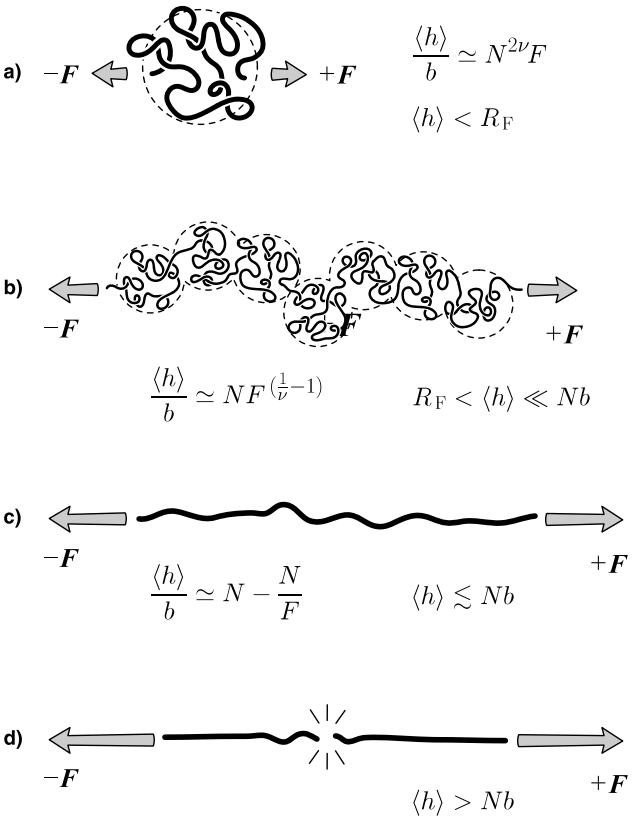

Figure 11. *Illustration of the four stretching regimes. a) The entropy of the polymer is able to keep both ends inside the Flory radius R_{F}. The forces applied to the polymer are too small to substantially deform it. This regime acts like an entropic spring and $\langle h^2\rangle/b$ scales as $N^{6/5}$ compared to N^1 for the FJC. b) The second regime is referred to as the Pincus regime. It corresponds to a stronger force which stretches the polymer beyond R_{F}. The polymer can then be treated as a series of "blobs"; the inside of the blobs is considered as a real chain while blobs are almost perfectly aligned. This regime predicts $\langle h\rangle \simeq F^{2/3}$ in 3 dimensions, but $\langle h\rangle \simeq N^1$ like the FJC model. c) In this regime the polymer is stretched to nearly full extension. We can treat it as an ideal chain since it is highly improbable that non-consecutive beads will interact with one another. d) The last regime occurs when one goes beyond an end-to-end distance of Nb. At this extension a polymer would be inclined to break into two subchains.*

2.6 Planar Perturbation in a Lennard-Jones Fluid

The present study is intended to examine a planar perturbation taking place in a Lennard-Jones fluid in terms of velocity, diffusion and absorption. There are several dissipation mechanisms like viscosity, heat conduction and relaxation taking place in a fluid. They are responsible for the amplitude reduction of sound waves. This phenomenon is different from the attenuation which takes place in a spherical wave field for example, which is a pure geometrical effect. As a result no energy is actually lost; instead it is spread over a larger area.

In our simulations a planar perturbation is propagated along the x-axis. Two different ways have been employed to simulate a planar perturbation. The first technique consists in displacing a plane of particles perpendicular to the x-axis by 0.3σ. The thickness of the plane is also 0.3σ. The second way is by giving an impulse to particles belonging to a plane of the same width. The first technique leads to an increase of both the kinetic and potential energy whereas the second produces an increase only in the kinetic energy. In both cases there will be a slight increase in the temperature of the system.

We have calculated the displacement amplitudes of fluid particles at different distances in the x direction from the perturbation source. To do so we have averaged the displacement amplitudes over all the atoms in planes of width 0.3σ along the x direction. Figure 12 shows the displacement amplitude profiles for each plane. The curves present a quasi-symmetrical bell-shaped distribution with a decreasing maximum as x increases. The width of the distribution increases as the perturbation moves away from the source. This indicates that the perturbation diffuses along its trajectory. The diffusing tail becomes more and more pronounced when one is far from the source. As noted earlier, the diffusion is due to the dissipation taking place in the fluid. At a microscopic level the dissipation can be interpreted as a slow redistribution of the perturbation energy among all the particles.

Although the planes are equally spaced, the maxima in Figure 12 are not, leading to an apparent non-constant velocity of the perturbation. That is why we cannot compute the perturbation velocity by a simple peak to peak distance measurement. These distributions can be fitted with the well known Gaussian distribution

$$\langle \Delta x(D,x,v,t)\rangle \sim \frac{1}{\sqrt{Dt}} \exp\left(-\frac{(x-vt)^2}{4Dt}\right) \qquad (11)$$

where D is the diffusion coefficient of the plane and v its velocity. From Eqn. (11) we can derive the arrival time of the maximum amplitude

$$t_{\max}(x) = \frac{D}{2v^2}\left[2\sqrt{\frac{1}{4}+x^2\frac{v^2}{D^2}}-1\right] \qquad (12)$$

We can approximate relation (12) for two extreme values of x. When $x \gg D/2v$, $t_{max}(x)$ can be expressed by $t_{max} \sim x/v$, and the peak is moving with the same velocity as the perturbation. Near the source, i.e., at $x \simeq 0$,

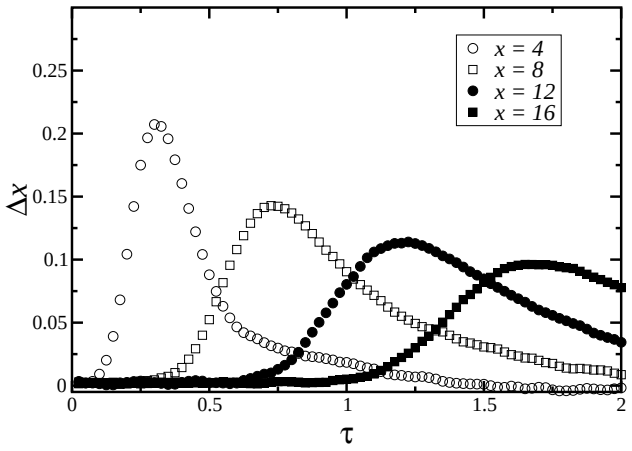

Figure 12. *Displacement amplitudes Δx of the perturbation at various positions from the source as a function of time τ. This simulations is carried out in a cube with $L = 41.8$ and reduced temperature $T^* = 1.1$.*

$t_{max} \sim x^2/2D$ and the peak movement is dominated by diffusion. We are currently looking at the measurement of fluid viscosity, the solvent diffusivity and the speed of sound using this novel approach. Our next step is to examine the effects of walls and polymers on this propagation phenomenon.

3 Conclusions and Remarks

With this survey of current projects, we have both illustrated the versatility of the Molecular Dynamics method to examine a wide variety of phenomena related to polymers in microenvironments and the scope of the research which our group is undertaking. We have hopefully illustrated the use of MD simulations in this regard.

4 Acknowledgements

The authors would like to thank the Natural Sciences and Engineering Research Council of Canada (NSERC) for a Research Grant to GWS. MK and SG also thank NSERC for a postgraduate scholarship and a postdoctoral fellowship respectively. MK, YG and FT thank the University of Ottawa for scholarships. YT would like to thank Materials Manufacturing Ontario (MMO-EMK) for funding. We would also like to acknowledge computational resources provided by the High Performance Computing Virtual Laboratory (HPCVL) and C3.ca.

References

1. R. G. Larson. Monte carlo simulation of amphiphilic systems in two and three dimensions. *J. Chem. Phys.*, 89(9):1642–1650, 1988.
2. R. G. Larson, L. Scriven, and H. T. Davis. Monte carlo simulation of model amphiphile–oil–water systems. *J. Chem. Phys.*, 83(5):2411–2420, 1985.
3. K. Zahn, R. Lenke, and G. Menke. Friction coefficient of rod-like chains of spheres at very low reynolds numbers. i. experiment. *J. Phys. II France*, 4:555–560, 1994.
4. K. Kremer and G. Grest. Molecular dynamics simulation for polymers in the presence of a heat bath. *Physical Review A*, 33(5):3628–3631, 1986.
5. K. Kremer, G. S. Grest, and I. Carmesan. Crossover from rouse to reptation dynamics: A molecular dynamics simulation. *Phys. Rev. Letters*, 61(5):566–569, 1988.
6. D. C. Rapaport. *The Art of Molecular Dynamics Simulation.* Cambridge University Press, 1995.
7. D. C. Rapaport. Molecular dynamics study of a polymer chain in solution. *J. Chem. Phys.*, 71(5):3299–3303, 1979.
8. K. Kremer and G. S. Grest. Dynamics of entagled linear polymer melts: A molecular dynamics simulation. *J. Chem. Phys*, 92(8):5057–5086, 1990.
9. M. P. Allen and D. J. Tildesley. *Computer Simulations of Liquids*. Oxford Science Publications, Oxford, 4^{th} edition, 1987.
10. S. J. Plimpton and B. A. Hendrickson. *Parallel Computing in Computational Chemistry*, chapter Parallel Molecular Dynamics Algorithms for Simulation of Molecular Systems, pages 114–132. American Chemical Society, Symposium Series 592, 1995.
11. M. Muthukumar. Translocation of a confined polymer through a hole. *Physical Review E*, 86(14):3188–3191, 2001.
12. M. Muthukumar. Polymer translocation through a hole. *Macromolecules*, 111(22):10371–10374, 1999.
13. J. K. Kasianowicz, E. Brandin, D. Branton, and D. W. Deamer. Characterization of individual polynucleotide molcules using a membrance channel. *Proc. Natl. Acad. Sci. USA*, 93:13770–13773, 1996.
14. Jeffrey Chuang, Yacov Kantor, and Mehran Kardar. Anomalous dynamics of translocation. *Physical Review E*, 65:011802, 2001.
15. O. B. Bakajin, T. A. J. Duke, C. F. Chou, S. S. Chan, R. H. Austin, and E. C. Cox. Electrohydrodynamic stretching of dna in confined environments. *Phys. Rev. Letters*, 80(12):2737–2740, 1998.
16. G. K. Batchelor. Slender-body theory for particles of abitrary cross section in stokes flow. *J. Fluid Mech.*, 44(3):307–312, 1970.
17. A. Meunier. Friction coefficient of rod-like chains of spheres at very low reynolds numbers. ii. numerical simulations. *J. Phys. II France*, 4:561–565, 1994.
18. A. E. Barron, H. W. Harvey, and D. S. Soane. A transient entanglement coupling mechanism for dna separation by capillary electrophoresis in ultradilute polymer solutions. *Electrophoresis*, 15:597–615, 1994.
19. B. Braun, H. W. Blanch, and J. M. Prausnitz. Capillary electrophoresis of dna restriction fragments: Effect of polymer properties. *Electrophoresis*, 18:1994–1997, 1997.
20. F. Han, B. H. Huynh, Y. Ma, and B. Lin. High–efficiency dna separation by capillary electrophoresis in a polymer solution with ultralow viscosity. *Anal. Chem*, 71(13):2385–2389, 1999.
21. P. S. Doyle, J. Bibette, A. Bancaud, and J. Viovy. Self–assembled magnetic matrices for dna separation chips. *Science*, 295(22):2828–2831, 2002.
22. P. André, D. Long, and A. Ajdari. Polyelectrolyte/post collisions during electrophoresis: Influence of hydrodynamics. *Eur. Phys. J. B*, 4(1):307–312, 1998.
23. E. M. Sevick and D. R. M. Williams. Long lived states in electrophoresis: Collision of a polymer chain with two or

more obstacles. *Euro. Phys. Letters*, 56(4):529–535, 2001.
24. W. B. Russel, D. A. Saville, and W. R. Schowalter. *Colloidal Dispersions*. Cambridge University Press, 1989.
25. S. Griffin and R. E. Majors. Fused-silica capillary – the story behind the technology. *Lc Gc N. Am.*, 20:928–938, 2002.
26. J. P. Gleeson. Electroosmotic flows with random zeta potential. *J. Colloid Interface Sci.*, 249:217–226, 2002.
27. C. L. Rice and R. Whitehead. Elektrokinetic flow in a narrow capillary. *J. Chem. Phys.*, 69:4017–4024, 1965.
28. A. T. Conlisk, J. McFerran, Z. Zheng, and D. Hansford. Mass transfer and flow in electrically charged micro- and nanochannels. *Anal. Chem.*, 74:2139–2150, 2002.
29. P. Dutta and A. Beskok. Analytical solution of time periodic electroosmotic flows: Analogies to stokes' second problem. *Anal. Chem.*, 73:5097–5102, 2001.
30. P. Dutta and A. Beskok. Analytical solution of combined eloectoossmotic/pressure driven flows in two-dimensional straight channels: Finite debye layer effects. *Anal. Chem.*, 73:1979–1986, 2001.
31. S. Z. Qian and H. H. Bau. A chaotic electroosmotic stirrer. *Anal. Chem.*, 74:3616–3625, 2002.
32. E. A. S. Doherty, R. J. Meagher, M. N. Albarghouthi, and A. E. Barron. Microchannel wall coatings for protein separations by capillary and chip electrophoresis. *Electrophoresis*, 24:34–54, 2003.
33. M. Deserno and C. Holm. How to mesh up ewald sums. i. a theoretical and numerical comparison of various particle mesh routines. *J. Chem. Phys.*, 109:7678–7693, 1998.
34. M. Deserno and C. Holm. How to mesh up ewald sums. ii. an accurate error estimate for the particle-particle-particle-mesh algorithm. *J. Chem. Phys.*, 109:7694–7701, 1998.
35. C. Sagui and T. A. Darden. Molecular dynamics simulations of biomolecules: Long-range electrostatic effects. *Annu. Rev. Biophys. Biomolec. Struct.*, 28:155–179, 1999.
36. P.-G. de Gennes. *Scaling Concepts in Polymer Physics*. Cornel University Press, Ithaca, 1979.
37. M. Doi and S. F. Edwards. *The Theory of Polymer Dynamics*. Oxford Science Publications, New York, 1986.
38. I. Teraoka. *Polymer Solution: An Introduction to Physical Properties*. John Wiley & Sons, Inc., New York, 2002.
39. G. W. Slater, S. J. Hubert, and G. I. Nixon. Construction of approximate entropic forces for finitely extensible nonlinear elastic (fene) polymers. *Macromolecular Theory and Simulation*, 3:695–704, 1994.